Eur. Phys. J. D **38**, 501–506 (2006)
DOI: 10.1140/epjd/e2006-00054-x

THE EUROPEAN PHYSICAL JOURNAL D

Projectile charge and velocity effect on UO_2 sputtering in the nuclear stopping regime

F. Haranger, B. Ban-d'Etat[a], Ph. Boduch, S. Bouffard, H. Lebius, L. Maunoury, and H. Rothard

Centre Interdisciplinaire de Recherche Ions Laser CIRIL, UMR 6637 (CEA, CNRS, ENSICAEN, Université de Caen), B.P. 5133, Boulevard Henri Becquerel, 14070 Caen Cedex 05, France

Received 24 May 2005 / Received in final form 6 December 2005
Published online 14 March 2006 –

Abstract. Angular distributions and yields of uranium sputtered by slow highly charged Xe^{q+} ions (kinetic energy 1.5 keV $\leq E_k \leq$ 81 keV, charge state $1 \leq q \leq 25$) from UO_2 were measured by means of the catcher technique. A charge state effect on the sputtering process is observed at 8 and 81 keV. A deviation from a $A\cos\theta$ shape (the linear collision cascade theory) is observed in case of Xe^{q+} impinging a UO_2 surface at $E_k = 8$ keV. Yields increase linearly with projectile charge state q thus clearly revealing the contribution of potential energy to the sputtering process. In addition, as the kinetic energy of a Xe^{10+} projectile decreases from 81 keV to 1.5 keV, a velocity effect is clearly observed on the angular distribution.

PACS. 34.90.+q Other topics in atomic and molecular collision processes and interactions – 61.80.Jh Ion radiation effects – 79.20.Rf Atomic, molecular, and ion beam impact and interactions with surfaces

1 Introduction

The interaction of slow ($v < v_0$, Bohr velocity $v_0 = 2.19 \times 10^6$ m/s) highly charged ions (SHI) with solid surfaces has been an active field of basic and applied research since many years [1–3]. Recent studies have stimulated interest in the application of SHI to surface characterization and materials modification on a nanometer scale. In this context, sputtering processes are an interesting way to understand the atomic motion induced by electronic excitations and elastic collisions in the solid targets.

Sputtering of surfaces by ion impact is a technique largely used as surface preparation. In this case, the kinetic energy of the projectile ion is used in order to dislodge the target atoms. Recently, more interest was directed to the effects of the projectile charge state on the sputtering process, and whether this can be exploited in more efficient surface preparation techniques. In order to enhance the projectile charge state effect on the sputtering process, mainly two possible paths can be chosen. The first path is by enhancing the projectile charge state. This choice is, however, relatively difficult, since the effects of kinetic and potential sputtering are mixed. To avoid this, the kinetic energy of the projectile ion was lowered, diminishing the effect of kinetic sputtering.

The energy loss per unit path length $(-dE/dx)$ of the projectile along its trajectory in the target material is the sum of two terms, the "nuclear stopping" $(-dE/dx)_n$ (elastic collisions between screened nuclei), and the "electronic stopping" $(-dE/dx)_e$ (excitation of target electrons). The mechanisms underlying sputtering processes due to the kinetic energy release of the projectile are consequently divided in two classes. They are defined as a function of the physical collision process involved: nuclear stopping is dominant at low kinetic energy of the projectile (less than 1 MeV) and leads to elastic collision cascades. Electronic stopping is dominant at high kinetic energy (larger than 1 MeV) and leads to "electronic sputtering". All the stopping power values given here have been calculated using the SRIM package software [4], which is standard for this purpose. While elastic sputtering is well described by theory, in the electronic sputtering regime several possible processes such as Coulomb explosion [5–7], thermal spike [8,9] and exciton production and migration mechanisms [10,11] are still under debate. In the case of SHI, initially far away from the equilibrium charge state, with kinetic energies of few keV, the distinction between "nuclear" and "electronic" sputtering is not relevant anymore. Both elastic collisions and intense electronic excitation occur simultaneously. Not only kinetic energy is released, but also the potential energy of the projectile (sum of the successive ionization energies) comes into play. Such a sputtering process is now referred to a "potential sputtering" [12]. Considering the time scale of interaction processes, it is admitted that the SHI neutralizes in a few femto-seconds close to the surface [6,13,14]. Therefore, the amount of its potential energy is initially deposited into the electronic system at the surface.

Several groups have studied sputtering yields for a variety of materials [5–23] with different charge states and

[a] e-mail: bandetat@ganil.fr

impact energies of the projectiles. Complementary models have been suggested to explain potential sputtering, in particular, for slow medium charge state projectile ions ($q < 28$) on insulators, Hayderer et al. [22] suggest a new mechanism termed as "Kinetically Assisted Potential Sputtering", KAPS. This refers to a potential sputtering which requires simultaneously the electronic excitation of the target material and the formation of collision cascade within the target (and therefore a minimum projectile kinetic energy) to initiate the sputtering process.

At very low kinetic energy (as low as $5q$ eV), Sporn et al. [17] have measured potential sputtering using a quartz crystal microbalance technique [12,13] with an error of few %. The catcher technique used by several authors allowed to determine the total sputtering yield with an uncertainty of about 50% only. This large error bar is due to the fact that assumptions about the shape of the angular distribution are necessary to calculate the total yield [2]. A strong enhancement of the sputtering yields with projectile charge state or potential energy has been observed for different targets. For Ar^{q+}, at 50–80 keV interacting with CsI, $LiNbO_3$ and Au, Weathers et al. [24] have measured the angular distribution, which follows a cosine law. A slight enhancement of the yields has been observed as the projectile charge state increases from 4+ to 11+.

We have previously measured angular distributions (AD) and total yields (Y) of uranium sputtered by slow highly charged Xe^{q+} ions (kinetic energy $E_k = 81$ keV, charge state $1 \leq q \leq 25$) at various incidence angles of the projectile [25]. The aim of these experiments was studying charge state and angle of incidence effects on the sputtering process. At 81 keV, the angular distributions were found to be non-isotropic and a clear charge state effect on the total sputtering yield was observed. In addition it was shown that going from normal to oblique incidence the sputtering yield increases in the beam forward direction.

To complete this study, we report here on measurements of both AD and yields of uranium sputtered by slow highly charged Xe^{q+} ions (kinetic energy 81 keV $\geq E_k \geq 1.5$ keV, charge state $1 \leq q \leq 25$). On one hand, by fixing the total projectile kinetic energy while varying its charge state, we investigate the effect of the potential energy on sputtering. On the other hand, by decreasing the projectile kinetic energy we get closer to the nuclear stopping regime, where the kinetic energy transfer relies on nucleus–nucleus interaction and depends mainly on the development of a more or less dense displacement cascade. Therefore, in order to separate the contributions of kinetic and potential energies, two set of experiments have been performed keeping constant either the projectile kinetic energy E_k at 8 keV and 81 keV (Xe^{1+}–Xe^{25+}) or the charge state (Xe^{10+}) while varying the kinetic energy between 81 keV and 1.5 keV.

2 Experiment

We used the catcher technique, which allows in particular the detection of neutrals, the large majority of the emitted particles. Far less than a percent of the sputtered particles are charged [26]. The ablated particles (neutrals, ions, clusters ...) are collected on a catcher made of low Z material placed in front of the target, which is in the center of the set-up. The beam passes through a 3 mm hole in the collector to hit the surface target at normal incidence. We used an ultra pure Al foil (99.999% Al) to collect the emitted particles, the sticking coefficient of which has been found close to unity [27]. The Al foil is curved in a hemispherical holder, the diameter of which is 20 mm. This experimental set-up has been described in a previous paper [25]. After irradiation, a step-by-step analysis of the collector by Rutherford Back scattering Spectrometry (RBS) allows the determination of the density of ablated uranium deposited on the Al foil, each position corresponding to an emission angle. These RBS analysis, used for the experiment done with projectiles at 81 keV, have been performed with 1.2 MeV He^+ ion beams delivered by a van de Graaff accelerator, at the "Centre de Spectrométrie Nucléaire et de Spectrométrie de Masse" (CSNSM, Orsay – France). In the case of irradiations at very low kinetic energies, the catchers were analyzed using a Heavy-Ion RBS (HIRBS) ensuring a better sensitivity than the RBS technique. This analysis has been performed with 3 MeV Ar^{2+} ions delivered by Ionen Strahl Labor (ISL) at the Hahn-Meitner-Institut HMI [28]. The sputtering yields are then deduced by integrating the doubly differential angular distributions $d^2Y/d\Omega$ over the angle of emission.

The targets used are sintered powders of uranium dioxide UO_2 prepared through a complete cycle of mechanical polishing and annealing using a reducing atmosphere (1400 °C, Ar/H_2) [29]. The surface roughness and grain size distributions was then measured using an Atomic Force Microscope (AFM), in order to validate the preparation process and control the similarity of the irradiated surfaces.

First, we study the charge state effect on the sputtering process. For this study a set of three experiments were necessary. In a first experiment, keeping constant the projectile kinetic energy at 81 keV, we vary the charge state q of xenon ions ($q = 10$, 15 and 25) corresponding to potential energies of 0.8 keV, 2.2 keV and 8 keV, respectively. The ions were extracted from the Electron Cyclotron Resonance Ion Source (ECR) at LIMBE (now, part of ARIBE, CIRIL-GANIL-Caen, France) with an acceleration voltage of 8.1 kV, 5.4 kV and 3.24 kV, respectively, to obtain a constant projectile kinetic energy of 81 keV. The singly-charged xenon ion beam at $E_k = 81$ keV was delivered by the source (IRMA) at the CSNSM (Orsay, France). In a third experiment, we study the charge state effect at a constant projectile kinetic energy equal to 8 keV. The beams of Xe^{10+}, Xe^{15+} and Xe^{25+} were extracted at 10 kV/q from the ECR source at HMI (Berlin, Germany) and then decelerated through an electrostatic lens system to 8 keV kinetic energy. For each AD measurement, the relative error of the fluence was estimated to be less than 5%; the fluency was kept roughly constant around 4×10^{14} ions on a surface of 0.28 cm^2.

Table 1. A, and n parameters, of equation (1), $A\cos^n\theta$, describing the Angular distribution of sputtered particles induced by Xe^{1+}, Xe^{10+}, Xe^{15+}, Xe^{25+} interacting with a kinetic energy of 81 keV.

q	A	n
1	0.52 ± 0.01	1.46 ± 0.1
10	0.63 ± 0.01	1.11 ± 0.07
15	0.72 ± 0.01	1.4 ± 0.05
25	0.88 ± 0.01	1.4 ± 0.06

It should be noted that we were not able to measure the AD for Xe^{1+} at 8 keV due to the stiffness of the beam, which cannot pass the selection magnets used with our ECR ion sources.

Second, to study the velocity effect a beam of Xe^{10+} was extracted at 10 kV/q from the ECR source at HMI (Berlin, Germany), fixing the charge state of the projectile while decelerating the beam through an electrostatic lens system to 8 keV, 5 keV and 1.5 keV kinetic energy.

3 Charge effect on UO_2 sputtering

The angular distributions of the ablated uranium obtained for Xe^{q+}, with q = 1, 10, 15, and 25 at 81 keV and 8 keV impinging the surface at normal incidence is presented in Figures 1a and 1b, where the angle $\theta = 0°$ corresponds to the direction perpendicular to the surface. Using this representation, an "isotropic" emission would result in a horizontal line. Consequently, the first main result is that, for any charge state at kinetic energies equal to 81 keV and 8 keV, the sputtering emission is strongly non-isotropic, and oriented preferentially along the surface normal.

At high kinetic energy, 81 keV, the AD of the sputtering follows a cosine law as predicted by the linear collision cascade [30]

$$A\cos^n\theta, \tag{1}$$

where the A and n parameters are given in Table 1.

This means that at 81 keV the shape of the angular distribution (i.e. the power n of the cosine function) does not present a clear variation with the charge state of the projectile. On the other hand, the A parameter strongly increases as the charge state of the projectile increases. This is the clear signature of an increasing of total sputtering yield, Figure 2. The sputtering yield, i.e. the number of sputtered U atoms per incoming projectile, is obtained by integration of the angular distribution over the emission solid angle.

At lower kinetic energy, 8 keV, a similar cosine law is observed for q = 10 and 15. Surprisingly an important deviation from the simple cosine law, equation (1), is observed for q = 25. The angular distribution may, in this particular case, be described by:

$$A\cos^n\theta + B\exp -\alpha\theta^2 \tag{2}$$

where the A, n, B and α parameters are given in Table 2.

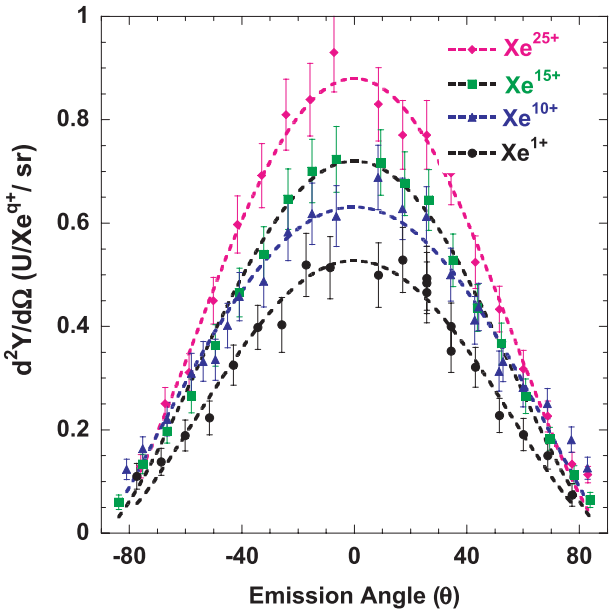

(a)

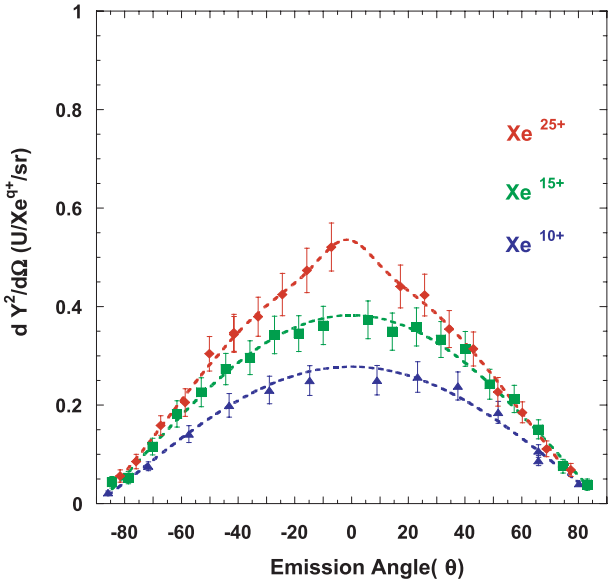

(b)

Fig. 1. Angular distributions $d^2Y/d\Omega$ (U/Sr/Xe^{q+}) of sputtered particles, versus the angle of emission (θ), induced by Xe^{1+}, Xe^{10+}, Xe^{15+}, Xe^{25+} interacting with a UO_2 surface at normal incidence with a kinetic energy of (a) 81 keV, (b) 8 keV. The lines are fit by equations (1) and (2) (see text).

Table 2. A, n, B and α parameters of equation (2), $A\cos^n\theta + B\exp -\alpha\theta$, describing the angular distribution of sputtered particles induced by Xe^{10+}, Xe^{15+}, Xe^{25+} interacting with a kinetic energy of 8 keV.

q	A	n	B	α
10	0.28 ± 0.02	1.06 ± 0.09	0	
15	0.38 ± 0.01	1.09 ± 0.06	0	
25	0.47 ± 0.02	1.26 ± 0.08	0.06 ± 0.04	12.2 ± 10.0

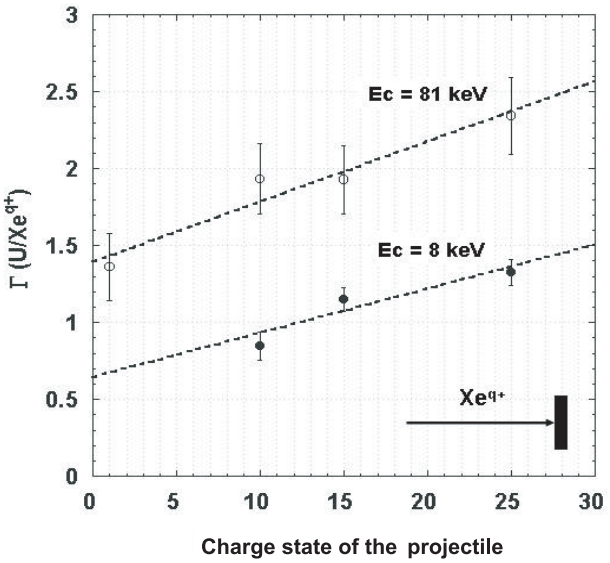

Fig. 2. Total sputtering yields Y (U/Xe^{q+}) presented as a function of the projectile charge. These results are obtained under the following conditions: Xe $^{10+,15+,25+}$ impinging a UO_2 target at 8 and 81 keV, Xe $^{1+}$ with $E_k = 81$ keV.

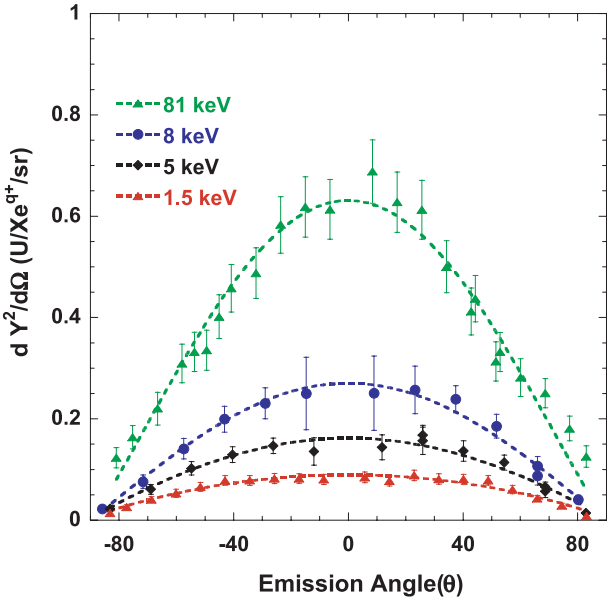

Fig. 3. Angular distributions $d^2Y/d\Omega$ (U/Sr/Xe^{q+}) of sputtered particles, versus the angle of emission (θ), induced by Xe^{10+} interacting with a UO_2 surface at normal incidence with kinetic energies equal to 81, 8, 5 and 1.5 keV.

Table 2, together with the corresponding Figure 1b, clearly underlines a charge effect on the angular distribution of sputtering and on the total yield at 8 keV: the power n of the cosine law increases as the charge state increases. We observe, as for $E_k = 81$ keV, an increasing value of the A parameter (i.e. the sputtering yield) with the charge state of the projectile, Figure 2. This enhancement amounts to about 30%, much larger than that presented in reference [24] (Ar^{q+} with $q = 4$, 8, 11 at 48 keV and 60 keV impinging on $LiNbO_3$ and CsI) where it is less than 10%. In addition, we note the linear increase with the charge state in accordance with the experimental results obtained by Schenkel et al. [2]. However, it should be kept in mind that their experimental conditions and sample preparation were different. In contrast to our experiments, this group has used an EBIT source, which can deliver very high charge state ions (from Xe^{27+} up to Th^{70+} with total kinetic energies ranging from 293 keV to 570 keV). The total sputtering yield was determined by the catcher method, but certain assumptions for the angular distributions had to be made [2].

4 Velocity effect on UO_2 sputtering

In a second experiment, we studied the projectile velocity effect on the sputtering process by fixing the charge state of the projectile (Xe^{10+}) impinging on the UO_2 target while decreasing its kinetic energy from 81 keV to 1.5 keV, Figure 3. The measurements with lower projectile velocities were performed using the ECR source at HMI. In Figure 3, the doubly differential sputtering yield $d^2Y/d\Omega$ (U/Sr/Xe^{q+}) is drawn as a function of the emission angle (θ). We present here, for the first time, the effect of the projectile velocity (Xe^{10+}) on the angular distribution of sputtered particles. At low kinetic energy (1.5 keV, 5 keV and 8 keV), the shape of the angular distribution changes significantly compared to higher projectile energy (81 keV). The maximum along the direction perpendicular to the surface disappears as the kinetic energy decreases. The AD follow the cosine law given by equation (1) with the parameters A and n given in Table 3.

Table 3. A, and n parameters, of equation (1), $A\cos^n\theta$, describing the angular distribution of sputtered particles induced by Xe^{10+} interacting with a kinetic energy of 1.5 keV, 5 keV, 8 keV and 81 keV.

E_k	A	n
81 keV	0.63 ± 0.01	1.11 ± 0.07
8 keV	0.27 ± 0.007	1.02 ± 0.07
5 keV	0.16 ± 0.006	0.88 ± 0.09
1.5 keV	0.08 ± 0.002	0.75 ± 0.06

At 1.5 keV, 5 keV projectile kinetic energy the shape is clearly flatter than the previous one at 8 keV and 81 keV. No preferential direction of the emitted particles is observed anymore at 0°. The variation of the power n of the cosine function indicates clearly that there is a velocity effect on the angular distribution in this regime.

Finally, let us have a look at the ratio of sputtering yields Y and the nuclear stopping power S_n. This ratio is plotted as a function of the projectile kinetic energy for Xe in UO_2 in Figure 4. The ratio is roughly constant for $E_{kin} < 81$ keV (i.e. in the nuclear stopping regime). However, the yields measured at LLNL are considerably higher than the yields measured at GANIL and HMI. Possible reasons may include an additional contribution to sputtering from electronic excitation and the higher potential energy. Also, the already above mentioned differences in

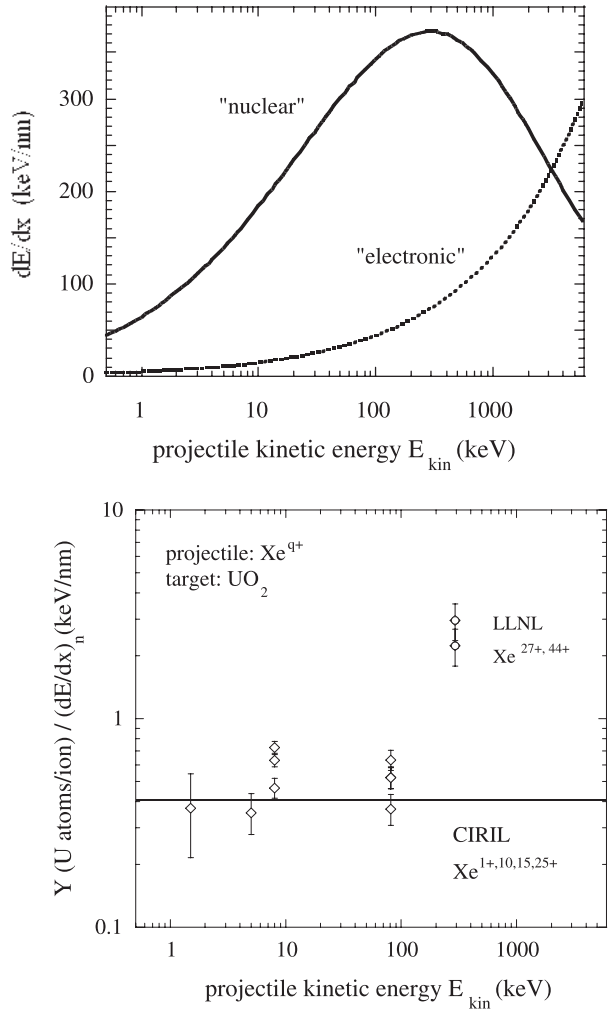

Fig. 4. Top: electronic and nuclear stopping power (more precisely, energy loss per unit path length, from [4]) as a function of projectile kinetic energy for Xe in UO_2. Bottom: ratio of sputtering yields Y and the nuclear stopping power S_n, as a function of projectile kinetic energy for Xe in UO_2. Lines are to guide the eye. Also included are data obtained by Schenkel et al. [2] at LLNL.

the procedure of determining the yields and different experimental conditions may come into play.

5 Discussion and outlook

In this experimental study, we measured angular distributions and sputtering yields of uranium sputtered from uranium dioxide UO_2 by slow highly charged Xe^{q+} ions. In case of $E_k = 81$ keV, the angular distribution, $A\cos^n\theta$, does not change with the charge state of the projectile, this first result might be predictable, taking into account that the projectile kinetic energy is still higher than potential energies, which are equal to 0.8 keV, 2.2 keV and 8 keV for Xe^{q+}, with $q = 10$, 15 and 25, respectively. Nevertheless, we observe an increase of the A parameter as the charge state increases, corresponding to an increase of the total sputtering yield. On the other hand, the study of the charge effect on the angular distribution, at a projectile kinetic energy equal to 8 keV, shows a deviation of the previous law, $A\cos^n\theta$, for a charge state $q = 25$. At this point, we might underline that the potential energy of the projectiles, Xe^{q+}, are not anymore negligible compared to the kinetic energy 8 keV ($E_p = 8$ keV for Xe^{25+}). We are clearly in the nuclear regime where the potential sputtering has to be considered. In addition, yields increase linearly with projectile charge q thus clearly revealing the contribution of potential energy to sputtering. Considering the behaviour of the yields with respect to the kinetic energy of the projectile and its charge state, the KAPS mechanism, [22], suggested for sputtering of insulators, might provide an explanation in our case with UO_2, which constitutes a semi conducting target [29].

In a second experiment, we studied the projectile velocity effect by fixing the charge state of the projectile ($q = 10+$) while varying the kinetic energy from 81 keV to 1.5 keV. Decreasing the projectile kinetic energy, the angular distribution becomes flatter, the maximum along the direction perpendicular to the surface disappears, a clear velocity effect is observable. For lower projectile kinetic energy, the angular distributions become difficult to measure due to the roughness of the sample surface. In our case, the roughness was measured with an AFM, and found to be less than 1.7 nm.

Together with our studies on the projectile incidence angle dependence of angular distributions [25], we now have obtained a rather large set of information on the sputtering of uranium dioxide by slow highly charged ions. In addition, our group has also measured the contribution of ionic species and clusters to sputtering [31]. Measurements of the cluster-size distribution of positively charge secondary ions from sputtering of uranium dioxide UO_2 by neon and argon ions ($q = 8$) and xenon ions of different charge states ($q = 10$, 23) at fixed kinetic energy (81 keV) were performed. The size-distribution of the cluster ion yields Y can be described by a power law $Y \sim n^{\delta}$ with δ-values between -1.5 and -2.9. This is in agreement with the predictions of collective models, but not with a statistical rearrangement upon exit.

Cluster emission contributes up to 70% of emitted uranium at 81 keV (positive secondary ions). An interesting and yet unsolved question is whether atoms, monomers, molecules and clusters have the same sputtering angular distribution. If the angular distribution of sputtered atoms and clusters is different, the appearance of additional components such as equation (2) to a pure cosine law equation (1) becomes plausible. Of course, also different physical mechanisms such as elastic collision cascade versus potential energy related or other electronic processes may be involved. In the first case, however, the yield of the different contributions should be connected to the contribution of monomers and clusters, respectively. In the second case, the footprints of the different physical mechanisms should be different angular and energy distributions of monomers and clusters, respectively. Possible ways to study this are XY-TOF-imaging techniques

for secondary ions [32]. For emitted neutrals, microscopic techniques used on the catchers may in some cases allow to separate emitted clusters from atoms (in particular for large clusters) [33]. Also, post-ionization techniques combined with XY-TOF may be a pathway to further investigating this question.

Fruitful collaborations and participations in the experiments of W. Bohne, R. Hellhammer, Z. Pešić, J. Röhrich, N. Stolterfoht and E. Strub (HMI-Berlin), C. Clerc, F. Garrido, S. Gautrot, O. Kaïtasov and L. Thomé (CSNSM-Orsay) and J.Y. Pacquet (GANIL-Caen) are gratefully acknowledged. We thank the support staff at the CIRIL and in particular, J.M. Ramillon, for their assistance in preparing for these experiments. This work was supported by the E.U. in the frame of the RTD project HITRAP, HPRI-CT-2001-50036 and part of the experiments were performed with the ion beam of the Grand Accélérateur National d'Ions Lourds (GANIL-Caen).

References

1. G. Betz, K. Wien, Int. J. Mass Spectrom. Ion Process. **140**, 1 (1994)
2. T. Schenkel, A.V. Hamza, A.V. Barnes, D.H. Schneider, Progr. Surf. Sci. **61**, 23 (1999)
3. R.A. Baragiola, Phil. Trans. R. Soc. Lond. A **362**, 29 (2004)
4. `www.srim.org`, based on *The Stopping and Range of Ions in Solids*, edited by J.F. Ziegler, J.P. Biersack, U. Littmark (Pergamon Press, New York, 1985; new edition in 2003)
5. I.S. Bitensky, M.N. Murakmetov, E.S. Parilis, Zhur. Tek. Fiz. SSSR **49**, 1044 (1979)
6. E.S. Parilis, Phys. Scripta T **92**, 197 (2001)
7. J. Burgdörfer, P. Lerner, F.W. Meyer, Phys. Rev. A **44**, 5674 (1991)
8. W.L. Brown, in *Ionisation of Solids by Heavy Particles*, edited by R.A. Baragiola (Pergamon Press, New York), NATO ASI Series B: Phys. **306**, 395 (1993)
9. M. Toulemonde, W. Assmann, C. Trautmann, F. Grüner, H.D. Mieskes, H. Kucal, Z.G. Wang, Nucl. Instr. Meth. B **212**, 346 (2003)
10. G. Hayderer, M. Schmid, P. Varga, H.P. Winter, F. Aumayr, L. Wirtz, C. Lemell, J. Burgdörfer, L. Hägg, C.O. Reinhold, Phys. Rev. Lett. **83**, 3948 (1999)
11. K. Mochiji, N. Itabashi, S. Yamamoto, H. Schimizu, S. Ohtani, Y. Kato, H. Tanuma, K. Okuno, N. Kobayashi, Surf. Sci. **357**, 673 (1996)
12. F. Aumayr, H.P. Winter, Phil. Trans. R. Soc. Lond. A **362**, 77 (2004)
13. S.T. de Zwart, T. Fried, D.O. Boerma, R. Hoekstra, A.G. Drentje, A.L. Boers, Surf. Sci. **177**, L939 (1986)
14. H. Winter, Phy. Rep. **367**, 387 (2002)
15. M. Hattass, T. Schenkel, A.V. Hamza, A.V. Barnes, M.W. Newman, J.W. McDonald, T.R. Niedermayr, G.A. Machicoane, D.H. Schneider, Phys. Rev. Lett. **82**, 4795 (1999)
16. G. Hayderer, M. Schmid, P. Varga, H.P. Winter, F. Aumayr, Rev. Sci. Instr. **70**, 3696 (1999)
17. M. Sporn, G. Libiseller, T. Neidhart, M. Schmid, F. Aumayr, H.P. Winter, P. Varga, M. Grether, D. Niemann, N. Stolterfoht, Phys. Rev. Lett. **79**, 945 (1997)
18. P. Varga, T. Neidhart, M. Sporn, G. Libiseller, M. Schmid, F. Aumayr, H.P. Winter, Phys. Scripta T **73**, 307 (1997)
19. K. Mochiji, S. Yamamoto, H. Schimizu, S. Ohtani, T. Seguchi, N. Kobayashi, J. Appl. Phys. **82**, 6037 (1997)
20. T. Schenkel, A.V. Hamza, A.V. Barnes, D.H. Schneider, J.C. Banks, B.L. Doyle, Phys. Rev. Lett. **81**, 2590 (1998)
21. T. Schenkel, A.V. Barnes, A.V. Hamza, D.H. Schneider, J.C. Banks, B.L. Doyle, Phys. Rev. Lett. **80**, 4325 (1998)
22. G. Hayderer, S. Cernusca, M. Schmid, P. Varga, H.P. Winter, F. Aumayr, D. Niemann, V. Hoffman, N. Stolterfoht, C. Lemell, L. Wirtz, J. Burgdörfer, Phys. Rev. Lett. **86**, 3530 (2001)
23. F. Aumayr, P. Varga, H.P. Winter, Int. J. Mass. Spect. **192**, 415 (1999)
24. D.L. Weathers, T.A. Tombrello, M.H. Prior, R.G. Stokstad, R.E. Tribble, Nucl. Instr. Meth. B **42**, 307 (1989)
25. B. Ban-d'Etat, F. Haranger, Ph. Boduch, S. Bouffard, H. Lebius, L. Maunoury, J.Y. Pacquet, H. Rothard, C. Clerc, F. Garrido, L. Thomé, R. Hellhammer, Z. Pešić, N. Stolterfoht, Phys. Scripta T **110**, 389 (2004)
26. A. Arnau, F. Aumayr, P. M. Echenique, M. Grether, W. Heiland, J. Limburg, R. Morgenstern, P. Roncin, S. Shippers, R. Schuch, N. Stolterfoht, P. Varga, T. Zouros, H.P. Winter, Surf. Sci. Rep. **27**, 113 (1997)
27. K.G. Libbrecht, J.E. Griffith, R.A. Weller, T.A. Tombrello, Rad. Eff. **49**, 195 (1980)
28. W. Bohne, G.-U. Reinsperger, J. Röhrich, G. Röschert, B. Selle, P. Stauß, Nucl. Instr. Meth. B **161–163**, 467 (2000)
29. F. Garrido, C. Choffel, L. Thomé, J.-C. Dran, L. Nowicki, A. Turos, J. Domagala, Nucl. Instr. Meth. B **136**, 465 (1998)
30. P. Sigmund, Phys. Rev. **184**, 383 (1969)
31. S. Boudjadar, F. Haranger, T. Jalowy, A. Robin, B. Ban d'Etat, T. Been, Ph. Boduch, H. Lebius, B. Manil, L. Maunoury, H. Rothard, Eur. Phys. J. D **32**, 19 (2005)
32. J. Lenoir, F. Haranger, S. Boudjadar, T. Jalowy, B. Ban-d'Etat, T. Been, P. Boduch, A. Cassimi, H. Lebius, B. Manil, L. Maunoury, H. Rothard, presented at *IRSIB-International Workshop on Interdisciplinary Research with Slow Ion Beams*, Caen, 9–11 October 2005, link: "Particle ejection from UO_2 by Xe^{q+}" at `http://www.ganil.fr/ciril/IRSIB/presentations.htm`
33. R.C. Birtcher, S.E. Donnelly, S. Schlutig, Phys. Rev. Lett. **85**, 4968 (2000)